Iranian Polymer Journal (2018) 27:1–11
https://doi.org/10.1007/s13726-017-0578-1

ORIGINAL PAPER

Hybrid silane-treated glass fabric/epoxy composites: tensile properties by micromechanical approach

Somayeh Safi[1] · Ali Zadhoush[1] · Mojtaba Ahmadi[2] · Sayed Pedram Rezazadeh Tehrani[1]

Received: 15 February 2017 / Accepted: 25 October 2017 / Published online: 14 November 2017

Abstract
The effect of interface modification on the interfacial adhesion and tensile properties of glass fabric/epoxy composites was evaluated in two directions of 0° and +45°. Herein, the glass fabric surface was modified by colloidal nanosilica particles and by a new blend of silane-coupling agents including both reactive and non-reactive silanes. Composite samples with high strength and toughness were obtained. A simultaneous improvement of tensile strength and toughness was observed for an epoxy composite reinforced with a hybrid-sized glass fabric including silane mixture and nanosilica. In fact, the incorporation of colloidal silica into the hybrid sizing dramatically modified the fiber surface texture and created mechanical interlocking between the glass fabric and resin. The results were analyzed by the rule of mixtures (ROM), Halpin–Tsai (H–T), and Chamis equations. It was found that the ROM equations provided approximate upper bound values for all investigated composite samples. In the samples containing nanosilica, the shear and elastic moduli values calculated by the Chamis and ROM equations showed good agreement with those obtained from experiments. However, in other samples, the values calculated by the H–T equation showed a better agreement with the experimental data. The analysis of fracture surfaces indicated that both silane and nanosilica particles had influence on the mode of failures at the interface.

Keywords Composite · Nanoparticle · Mechanical properties · Interfaces · Models

Introduction

Nowadays, composites and nanocomposites have shown promising features including electrical, mechanical, and thermal properties in different applications such as sports goods, aerospace fields and automotive industries [1–4]. Fiber-reinforced composites can be fabricated with different types of fibers, namely carbon, Kevlar, and glass fibers. Glass fibers, as cost-effective reinforcements, possess outstanding merits such as high tensile strength, great chemical resistance, and excellent insulating property [5–8]. Fiber-reinforced polymer composites have attracted great attention in the last 30 years, compared with common structural materials, namely steel and aluminum. Such progress comes from their high strength and stiffness as well as light weight. The reason for this superior performance is ascribed to the synergistic effect stemming from the symbiosis of multi-scale constituents, e.g., micro- and nano-reinforcements. It is also hypothesized that this synergy is related to the interactions between fibers and polymeric matrixes [7, 9, 10].

It is well-known that the interphase plays a predominant role in determining interfacial-related properties of composites. For instance, a strong interfacial adhesion can efficiently transfer stress from the matrix to fibers, playing a key role in the determination of mechanical performance as well as guaranteeing the reliability [11–13]. There are two effective approaches to improve the adhesion between resin and glass fibers: micromechanical interlocking and chemical bonding which can support and promote composite properties [14–18]. It is supposed that mechanical attachments are introduced into the interphase by incorporation of nanoparticles into the sizing composition, wherein silane is capable of enhancing the interphase through chemical interactions [19–21].

A wide range of studies have been devoted to offer methods for tailoring fiber–matrix adhesion, which results in desired composite properties. Nonetheless, increasing the

✉ Ali Zadhoush
zadhoush@cc.iut.ac.ir

[1] Department of Textile Engineering, Isfahan University of Technology, Isfahan 84156/83111, Iran

[2] Institute for Frontier Materials, Deakin University, Geelong, VIC 3216, Australia

strength of fiber-reinforced polymer composite is often accompanied by a decrease in the toughness of composite material [12, 22, 23]. The combination of physical and chemical bonding is considered as a preferred way for establishing an optimal epoxy resin/glass fiber interface [14, 23, 24].In this regard, Jensen and McKnight [24] applied commercial sizing mixtures containing colloidal silica, on the surface of glass fibers using a single-step process. They found that the sizing increased impact energy absorption, while the structural properties of pultruded glass fiber-reinforced composites did not change. Gao et al. [14] modified the interphase by creating mechanical interlocking between the fibers and resin using silane blends, resulting in an increase in the surface roughness of the fibers as well as the energy absorption.

The focus of this work was to modify the surface of glass fiber using colloidal nanosilica and innovative mixtures of silane-coupling agents containing both reactive and non-reactive agents towards the matrix phase. The purpose was to obtain a composite, in which tensile strength and toughness were improved simultaneously. Due to the complexity of the sizing package, silane and nanoparticles were merely utilized in a model system to study the effect of texturing and chemical bonding on interphase properties [25–27].

In this work, γ-methacryloxypropyltrimethoxysilane (MPS) and 3-glycidoxypropyltrimethoxysilane (GPS) were used for the fiber surface treatment. In addition to incorporation of silica nanoparticles and GPS, an incompatible silane-coupling agent (MPS) was also added to the fiber sizing for controlling the density of reactive sites. These sites allowed the formation of chemical bonds with epoxy resin molecules. Due to the presence of MPS in hybrid sizing packages, it was expected that the chemical bonds between hybrid-sized fibers and resin were weaker than those of the compatible-sized glass fibers. It was reported [28] that due to the very strong chemical bonding between fibers and epoxy resin, the crack probably penetrated through the bulk of matrix. In this case, there were not any mechanical interlockings at the interphase for improvement of energy absorption capacity and strength [14].

Composite samples were prepared using glass fibers treated with silane sizing mixtures. Then the tensile properties (strength, modulus, and toughness) of the samples were measured. Tensile tests at 0° and +45° directions were used to validate specifications, quality assurance of specimens and failure modes. Additionally, tensile tests were used for research and development as well as testing strength and modulus to support the components of the project [29]. The rule of mixtures (ROM), Halpin–Tsai (H–T) and Chamis equations were used to analyze the experimental data.

Theoretical predictions

Elastic properties of unidirectional fiber lamina

The most widely used equations to predict mechanical properties of composites are the rule of mixtures (ROM), Chamis and Halpin–Tsai (H–T) equations. In these equations, it is assumed that the distribution of resin in the composite is uniform and the average fiber volume fraction in each ply is the same as the total fiber volume fraction. The elastic properties of unidirectional glass fiber lamina were predicted using a simple ROM from the mechanical properties of fiber and resin as follows [30, 31]:

$$E_1 = V_{\mathrm{f}}E_{\mathrm{f}} + V_{\mathrm{m}}E_{\mathrm{m}} \tag{1}$$

$$E_2 = E_{\mathrm{f}}E_{\mathrm{m}}/(V_{\mathrm{f}}E_{\mathrm{m}} + V_{\mathrm{m}}E_{\mathrm{f}}) \tag{2}$$

$$G_{12} = G_{\mathrm{f}}G_{\mathrm{m}}/(V_{\mathrm{f}}G_{\mathrm{m}} + V_{\mathrm{m}}G_{\mathrm{f}}) \tag{3}$$

$$\nu_{12} = V_{\mathrm{f}}\nu_{\mathrm{f}} + V_{\mathrm{m}}\nu_{\mathrm{m}} \tag{4}$$

where υ, V, E, and G are the Poisson's coefficient, fiber volume fraction, Young's modulus, and shear modulus, respectively (the subscripts f, m, 1 and 2 denote fiber, matrix, longitudinal, and transverse, respectively).

The Chamis micromechanical model is the most trusted model which gives a single formula for all independent elastic properties. It is noticed that E_1 and ν_{12} are also predicted in the same manner as the ROM model (Eqs. 1, 4), while for other moduli, V_{f} is replaced by its square root [31]

$$E_2 = E_{\mathrm{m}}/(1 - \sqrt{V_{\mathrm{f}}}(1 - E_{\mathrm{m}}/E_{\mathrm{f}})) \tag{5}$$

$$G_{12} = G_{\mathrm{m}}/(1 - \sqrt{V_{\mathrm{f}}}(1 - G_{\mathrm{m}}/G_{\mathrm{f}})) \tag{6}$$

The H–T model also emerged as a semi-empirical model for correcting the transverse modulus (E_2) and shear modulus (G_{12}). However, for E_1 and ν_{12}, the ROM model is used (Eqs. 1, 4) as follows [31, 32]:

$$M/M_{\mathrm{m}} = (1 + \xi\eta V_{\mathrm{f}})/(1 - \eta V_{\mathrm{f}}), \quad \eta = ((M_{\mathrm{f}}/M_{\mathrm{m}}) - 1)/((M_{\mathrm{f}}/M_{\mathrm{m}}) + \xi) \tag{7}$$

where M represents the composite moduli (the subscripts 'f' and 'm' denote fiber and matrix, respectively), V_{f} is the fiber volume fraction, and $\xi$is a measure of reinforcement for composite material and depends on the fiber geometry, packing geometry, and loading conditions ($\xi = 1$ and 2, for E_2 and G_{12}, respectively).

Elastic properties of woven fabric lamina

The woven fabrics were formed by fibers arranged along two mutually perpendicular directions: warp direction (the length direction of the woven fabric roll), and weft direction. The approximate values of fabric elastic properties consisted of two unidirectional plies crossing at 90° angle, either separately or together. The k factor, a required constant for determination of elastic properties of plain-woven ply, is defined as [30]:

$$k = n_1/(n_1 + n_2) = 0.5 \tag{8}$$

where n_1 is the number of warp yarns per meter and n_2 is the number of weft yarns per meter. Mechanical properties of these plies (E_x, E_y, G_{xy}, and υ_{xy}) are determined according to the following equations.[30]:

$$E_x \approx kE_1 + (1-k)E_2 \tag{9}$$

$$E_y \approx (1-k)E_1 + kE_2 \tag{10}$$

$$G_{xy} = G_{12} \tag{11}$$

$$\upsilon_{xy} \approx \upsilon_{12}/\left[k + ((1-k)E_1/E_2)\right] \tag{12}$$

where x and y are the warp and weft directions of the fabric, respectively.

The fabrics are said to be balanced, when there are as many warps as weft yarns with the same material. Therefore, the warp and weft directions play equivalent roles, concerning mechanical characteristics. Additionally, the elastic moduli in longitudinal and transverse directions are equal ($E_x = E_y$). The elastic modulus of a composite (E_c) is given by the following equation [30]:

$$E_c = 0.5 \times (E_1 + E_2) \tag{13}$$

where E_1 and E_2 are the elastic moduli, derived from longitudinal and transverse fibers, respectively.

The H–T equations needed to be modified concerning calculations of the elastic modulus of woven fabric-reinforced composites. Woven fabrics were considered to have two separate types of fibers, i.e., longitudinal and transverse with a volume fraction of $V_f/2$ for each type (where V_f was the reinforcement volume fraction). H–T equations could then be written as the following equation [33]:

$$E_c = F_1(E_1 + E_2) = F_1\left\{\left[E_m(1 + \xi_L\eta_L V_f/2)/(1 - \eta_L V_f/2)\right] + \left[E_m(1 + \xi_t\eta_t V_f/2)/(1 - \eta_t V_f/2)\right]\right\} \tag{14}$$

where E_c is the elastic modulus of the composite and F_1 is an empirical correlation function determined based on the differences between the experimental and calculated data. Theη_L and η_t are the parameters calculated with substitution of empirical parameter ξ_L (= 2 for longitudinal direction), and empirical parameter ξ_t (= 0.5 for transverse direction) in Eq. 7 [33].

Experimental

Materials

Commercially available woven roving E-glass fabric EWR400 with an area weight of 400 ± 20 g/m^2 and a thickness of 0.775 ± 0.04 mm was supplied by Sonmez Textile Advanced (Turkey). The silane materials included 3-glycidoxypropyltrimethoxysilane (GPS, M_w = 236.4, Merck, Germany), and γ-methacryloxypropyltrimethoxysilane (MPS, M_w 248.35, Merck, Germany). Ludox TMA (Merck, Germany) silica nanoparticles with an average dimension of 22 nm were suspended in deionized water (34 wt%) and used. Epoxy was chosen as a matrix system for the composites. A room temperature-cured epoxy resin EPOLAM 2017 and polyamine hardener EPOLAM 2018 were supplied by Axson, France (E_m = 2.2 GPa, G_m = 0.81 GPa). Resin/curing agent weight ratio at 100:30 was used for sample preparation.

Silane treatment of glass fabric

Before use, all organic materials were removed from the glass fabric surface using an air-circulating oven at 450 °C for 1.5 h [5]. Four different glass fiber sizing formulations containing combinations of silane-coupling agents and colloidal silica particles were applied to E-glass fabrics (according to Table 1).

The sample G contains the compatible silane-coupling agent GPS which controls the chemical bonding between the glass fiber and the epoxy resin matrix. The sample M contains only MPS, which is an incompatible silane with no chemical reactivity towards the epoxy-based matrix. A silane treatment involving the mixture of GPS and MPS was used to control the density of compatible reactive groups on the glass fabric surface (sample G1M1). A hybrid fiber sizing package consisting of a mixture of GPS, MPS, and the

Table 1 Formulations of designed fiber sizing mixtures

Sample code	Sizing formulation
G	0.5% GPS[a]
M	0.5% MPS[b]
G1M1	0.5% GPS + 0.5% MPS
G1M1-NP	0.5% GPS + 0.5% MPS + 1% NP

[a] 3-Glycidoxypropyltrimethoxysilane (GPS); compatible silane-coupling agent

[b] γ-Methacryloxypropyltrimethoxysilane (MPS); incompatible silane-coupling agent

colloidal silica as fiber surface roughening agent was used to create texture on the fiber surface (sample G1M1-NP).

To prepare a silane solution, a specified amount of silane (1 wt% silica solution) was added to a 75/25 (v/v) solution of ethanol and deionized water with a pH adjusted to 4.0 using acetic acid before mixing. The solution was stirred for 1 h at room temperature to complete hydrolysis of silane. Each fabric specimen was dipped into the silane solution for 15 min. Following that, the samples were air-dried overnight at room temperature and then heated to 110 °C for 1 h to allow complete condensation of the silanol groups and to promote the cross-linking process.

Composite panel fabrication

All composites were prepared by simple hand lay-up method in a mold at ambient temperature. A thin layer of wax was applied to the surface of the mold. Afterward, the epoxy resin and hardener (in a mixing ratio of 100:30 by weight) were stirred manually for 10 min. Then, the mixture was kept in a vacuum oven at 30 °C and 0.65 bar pressure for 15 min to eliminate air bubbles. The composite panel was prepared by impregnating woven fabric with epoxy resins using a hand roller. The laminate was cured for 36 h at room temperature, followed by post-cure for 2 h at 45 °C, 2 h at 60 °C, and 8 h at 80 °C in a vacuum oven. The composite samples were named according to the fabric codes (Table 1).

Tensile test of a single fiber

The tensile properties of glass fibers were measured using a Zwick Universal Testing machine (model-1446 60, Germany) according to ASTM D3379-75. The first step in the determination of the mechanical properties of the glass fibers was the measurement of a single filament diameter. The diameter measured by an optical microscope on more than 30 elementary filaments led to an average diameter of 15 ± 1.2 µm. Each elementary filament was bonded with a cyanoacrylate-based adhesive on a stiff paper frame to facilitate handling of filaments. After clamping the paper frame in the grips of the tensile testing machine, its midsection was cut. The tensile tests were carried out in the tensile machine with a 20-N load cell. The load was applied through a crosshead displacement of 0.5 mm/min. In each case, tensile strength was measured for 40 test specimens to obtain statistically meaningful results.

Physical properties of glass fabric/epoxy composite panels

General physical characteristics of the fabricated composite panels were measured. To determine the density of a composite panel, each was cut into a 1″ × 1″ dimension. The dry weight, W_1 (in the air), and the wet weight, W_2 (in the water), of the samples were measured. The composite density was then calculated using ASTM D792-98 dry/wet weight method as in the following equation:

$$\rho_{\mathrm{ce}} = W_1/(W_1 - W_2) \tag{15}$$

The actual fiber volume fraction was calculated from the fiber weight fraction determined experimentally according to ASTM D2584 (the ignition loss method) as in the following equation:

$$V_{\mathrm{f}} = (W_{\mathrm{f}}/\rho_{\mathrm{f}})/\left[(W_{\mathrm{f}}/\rho_{\mathrm{f}}) + (W_{\mathrm{m}}/\rho_{\mathrm{m}})\right] \tag{16}$$

where W_{f} is the fiber weight fraction (same as the fiber mass fraction); W_m is the matrix weight fraction (same as the matrix mass fraction) and is equal to $(1 - W_{\mathrm{f}})$; ρ_{f} and ρ_{m} are the fiber and matrix densities, respectively. The void content (V_{v}) in a composite sample is estimated by comparing the theoretical density (ρ_{ct}) with its actual density (ρ_{ce}) [32]:

$$v_{\mathrm{v}} = (\rho_{\mathrm{ct}} - \rho_{\mathrm{ce}})/\rho_{\mathrm{ct}} \tag{17}$$

$$\rho_{\mathrm{ct}} = 100/\left[(W_{\mathrm{f}}/\rho_{\mathrm{f}}) + (W_{\mathrm{m}}/\rho_{\mathrm{m}})\right] \tag{18}$$

where ρ is the density, W is the weight percentage, and V_{v} is the void content (the subscripts '*c*', '*f*', '*m*', '*e*' and '*t*' denote the composite, fiber, matrix, experimental and theoretical, respectively).

Tensile properties of composite panels

The tensile properties of glass fabric/epoxy composite samples were determined according to the ASTM D 3039 testing method. Three specimens, each with a dimension of 150 × 25 × 1.5 mm^3 were tested for each condition. The samples were prepared by bonding the end-tabs of the glass fiber/epoxy laminates. The tests were performed by a universal testing machine (Hounsfield Equipment, UK) equipped with a hydraulic grip and an extensometer at a constant speed of 2 mm/min at room temperature.

In-plane shear test

Shear strength and shear modulus were determined by a ± 45° shear test based on ASTM D3518. In this method, uniaxial tensile loading was applied to each specimen having warp fibers oriented at ± 45°. The load cell and rate of loading were the same as those of the tension test. The shear modulus G_{12} was determined from the slope of the linear portion of stress–shear plot.

SEM observation

After tensile tests, the fracture surface of the composites was characterized using a scanning electron microscope (SEM;

KYKY-EM3200, China). The fractured composite specimens were loaded on the SEM mount with double-sided electrically conductive adhesive carbon tape. The specimen mounts were coated with a thin layer of gold in an automatic sputter coater (KYKY-SBC 12, China) before the examination. The coated specimens were observed using an accelerating voltage of 25 kV.

Results and discussion

Tensile properties of glass fibers

The mechanical performance of glass fibers, in general, depends on many factors stemming from glass composition and its formation history. Tensile test results of the glass fibers before and after silane treatment of the fiber surface are shown in Table 2. The results showed that the tensile strength for as-received glass fibers was considerably lower than that of the theoretical expectation. This was attributed to the existence of surface defects, which could cause stress concentration and thus premature fracture as the fiber was loaded [32]. After heat-cleaning process (unsized sample), both tensile strength and failure strain of the glass fibers significantly decreased. This was due to the surface defects introduced to the etched fiber surface during the removal of the sizing material. However, there was no distinct variation in tensile modulus of the glass fibers. Statistical analysis was carried out by one-way analysis of variance (ANOVA) and Duncan's test at a significance level of 0.05. The results of Duncan's test analysis are shown in Table 2.

After silane treatment, both tensile strength and failure strain of the glass fibers increased, compared with the unsized ones. In fact, the silane-coupling agents affected fiber strength. It was reported that silanes seemed to have the ability to heal the surface defects and to improve the fiber strength. These multifunctional species could partially patch up the defects which orderly reduced the stress concentration in them [21, 34].

Physical properties of composite panels

The physical properties of glass fabric/epoxy composite panels, such as actual (experimental) density, theoretical density, void content, fiber weight fraction, and fiber volume fraction data are reported in Table 3. The experimental density was calculated according to ASTM D 792-98. The fiber volume fraction of composite was calculated by determination of the weights of the fiber and matrix, and the volumes of the fiber and matrix (ASTM D 2584).

Tensile properties of composite panels

The tensile test results for epoxy composite panels reinforced with unsized- and silane-treated glass fabrics are presented in Table 4. Work-up-to-break which is equal to force–deformation plot area of tensile curve was measured as the composite toughness. All results were normalized based on the

Table 2 Tensile properties of different glass fibers

Sample code	Tensile strength (MPa)	Tensile modulus (GPa)	Strain-at-break (%)
As-received	1091.01 ± 105.81^{d}	71.02 ± 7.02^{b}	2.15 ± 0.18^{A}
Unsized	526.68 ± 36.92^{a}	71.30 ± 6.10^{b}	0.85 ± 0.10
G	787.71 ± 65.90^{c}	$67.43 \pm 5.64^{a,b}$	2.00 ± 0.31
M	$737.80 \pm 59.67^{b,c}$	$83.29 \pm 4.93^{c,d}$	1.17 ± 0.11
G1M1	702.72 ± 69.93^{b}	$69.40 \pm 6.57^{a,b}$	1.50 ± 0.16
G1M1-NP	718.85 ± 69.87^{b}	88.18 ± 9.23^{d}	1.07 ± 0.15

[a,b,c,d,e] Means with the same superscript are not statistically different ($P < 0.05$)

[A] Mean ± Std. deviation

Table 3 Physical properties of glass fabric/epoxy composite panels

Sample code	Actual density, ρ_{ce} (g/cm^3)	Theoretical density, ρ_{ct} (g/cm^3)	Void content, V_v	Fiber weight fraction, W_f	Fiber volume fraction, V_f
Unsized	1.32 ± 0.014^{a}	1.39 ± 0.031	0.051 ± 0.011	0.32 ± 0.013	0.178 ± 0.004
G	1.40 ± 0.016	1.46 ± 0.010	0.042 ± 0.004	0.40 ± 0.018	0.240 ± 0.008
M	1.37 ± 0.019	1.43 ± 0.016	0.045 ± 0.002	0.37 ± 0.014	0.214 ± 0.005
G1M1	1.30 ± 0.013	1.37 ± 0.019	0.054 ± 0.004	0.30 ± 0.016	0.186 ± 0.003
G1M1-NP	1.34 ± 0.012	1.38 ± 0.023	0.042 ± 0.002	0.33 ± 0.010	0.171 ± 0.010

[a] Mean ± Std. deviation

highest fiber volume fraction of composite specimens (24%, Table 3) [35]. One-way analysis of variance (ANOVA) and Duncan's test (for multiple comparisons between means to determine significant differences) were used at a significance level of 0.05 for analyzing the experimental data.

Mechanical properties of a fiber/matrix composite not only depend on the properties of each primary component, but also on the nature of the fiber surface, the bond between fibers and resin, and the mechanism of load transfer at the interface/interphase [32].

According to Table 4, the compatible sizing (G) increased the tensile strength by 42% compared to that of incompatible sizing (M), due to the presence of reactive silane-coupling agents on the fiber surface. It was important to embed compatible silane-coupling agents in the fiber sizing materials and create certain chemical bonding between fiber and resin to achieve applicable strength properties. Compared to sample G, the sample M showed a lower work-up-to-break (toughness) value. This was ascribed to the poor adhesion of fiber to epoxy matrix in the sample M. In other words, the fiber pull-out mechanism and interfacial debonding could dissipate the energy of crack, resulting in higher energy absorption and toughness [36]. Therefore, when the interfacial adhesion between the fiber and the matrix was strong, much more energy was needed to pull out the fibers from the embedded matrix. Hence, the fiber movements due to modification were restricted [37, 38]. In the mixed sizing (sample G1M1), the presence of incompatible silane may dilute the concentration of reactive functional groups presented by compatible silane-coupling agents on the fiber surface. Consequently, the available bonding sites decreased, and the strength reduced slightly (3%). However, the toughness results showed an enhancement of about 3% in sample G1M1 in comparison to sample G.

The G1M1-NP sample exhibited the highest tensile strength and failure strain compared to the other composite panels. Moreover, a noticeable increment of 76 and 184% in the toughness of the G1M1-NP sample was observed compared to that of the G1M1 and G samples, respectively. These observations can be explained by energy dissipation mechanisms in fibers and silica nanoparticles pull-out during fracturing. In addition, the crack retardation was considered as another mechanism responsible for this increment. When the composite sample fails, the crack cannot directly pass through the interface due to the existence of silica nanoparticles in the interphase, which forms mechanical interlocking between the fiber and resin. In other words, an adhesive fracture changes to a cohesive fracture, penetrating into the bulk of the matrix [39–44]. This causes redistribution of the stress at the fiber/resin interface and more energy dissipation during the failure. In fact, hybrid sizing could increase both the strength and energy absorption. Figure 1 shows the stress–strain curves for different composite panels. These curves are nearly linear as expected for a brittle material. The G1M1-NP composite sample exhibits ductile behavior, which is reflected in its high strain-at-break compared to that of the other samples.

After the tensile tests, the specimens were photographed for further observation of failure patterns. Figure 2 shows failure modes of composite specimens treated with different sizing mixtures after the test. The unsized and M samples show that the crack propagation follows a straight line, similar to the brittle fractures (Fig. 2a, c), and thus a catastrophic

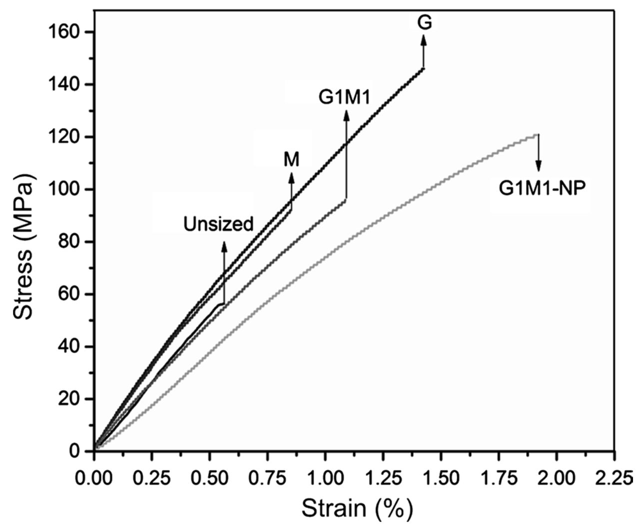

Fig. 1 Stress–strain curves of epoxy composites reinforced with the glass fabric treated with different silane sizing mixtures (sample codes are according to Table 1)

Table 4 Tensile properties of glass fabric/epoxy composite panels

Sample code	Tensile strength (MPa)	Tensile modulus (GPa)	Strain-at-break (%)	Toughness (N mm)
Unsized	84.97 ± 2.75^{a}	10.7 ± 0.14^{c}	0.55 ± 0.1^{A}	381.45 ± 15.26
G	145.36 ± 3.62^{d}	12.3 ± 0.27^{d}	1.42 ± 0.5	1191.70 ± 45.28
M	102.56 ± 1.33^{b}	11.7 ± 0.75^{d}	0.85 ± 0.1	626.07 ± 24.41
G1M1	141.24 ± 2.85^{c}	$9.91 \pm 0.72^{b,c}$	1.09 ± 0.1	1225.89 ± 52.71
G1M1-NP	153.50 ± 3.11^{e}	9.42 ± 1.05^{b}	1.92 ± 0.5	3384.25 ± 104.91

^{a,b,c,d,e} Means with the same superscript are not statistically different ($P < 0.05$)

^{A} Mean ± Std. deviation

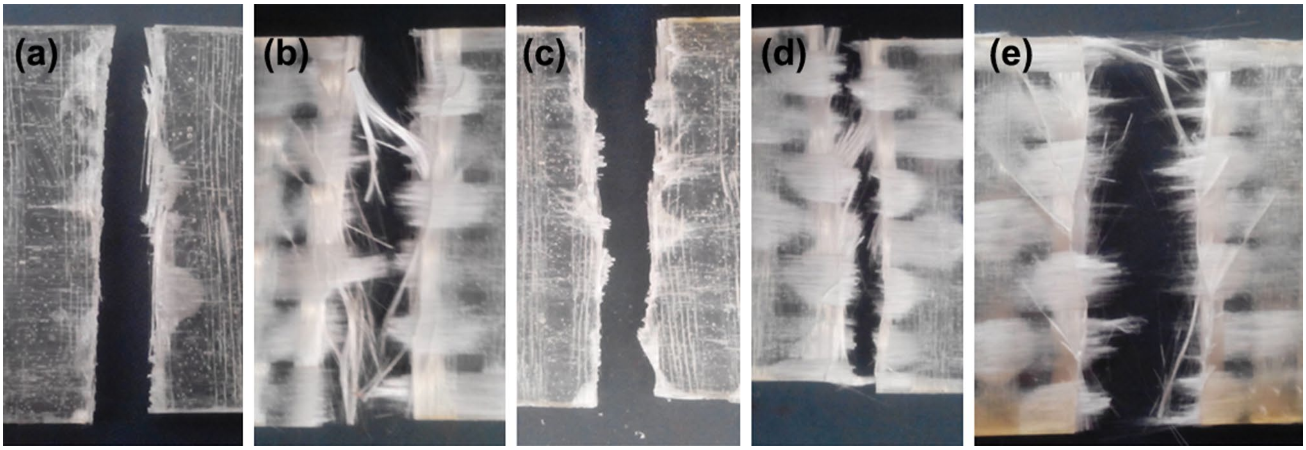

Fig. 2 Fracture type after tensile testing for samples: **a** unsized, **b** G, **c** M, **d** G1M1, and **e** G1M1-NP (sample codes are according to Table 1)

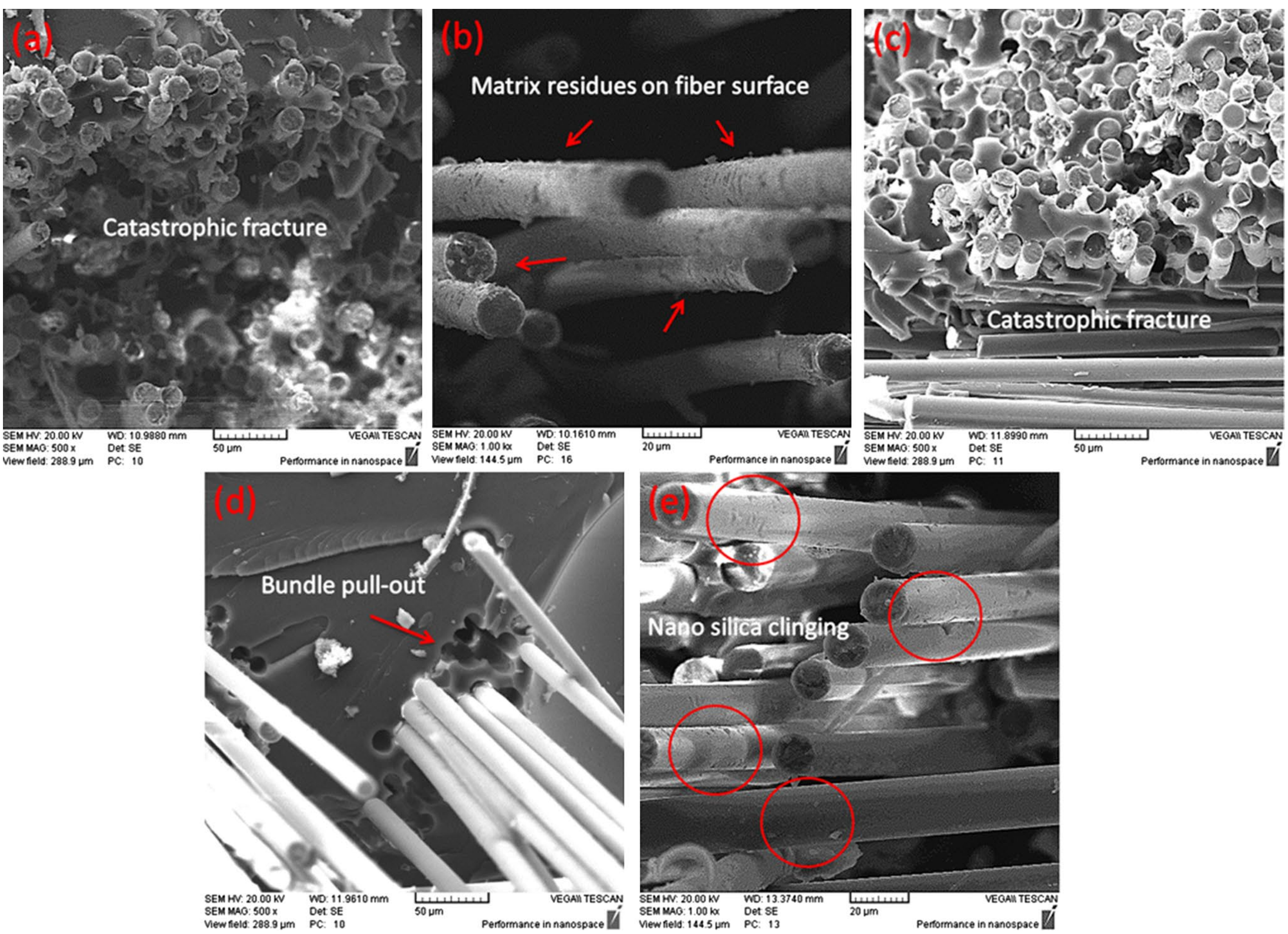

Fig. 3 Fracture surface micrographs (×500 and ×1000) of glass fiber/epoxy composites after tensile test for samples: **a** unsized, **b** G, **c** M, **d** G1M1, and **e** G1M1-NP (sample codes are according to Table 1)

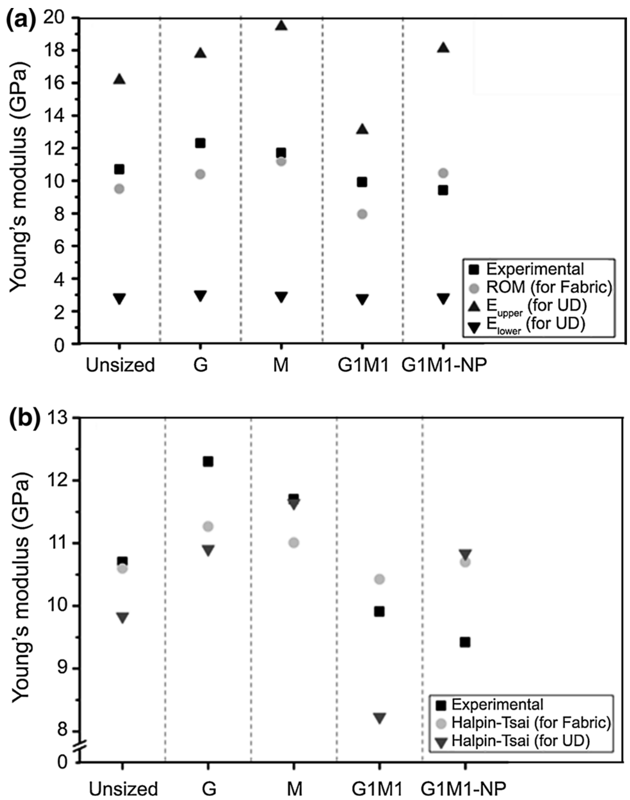

Fig. 4 Application of: **a** ROM, and **b** Halpin–Tsai (H–T) equations to experimental data for Young's modulus (sample codes are according to Table 1)

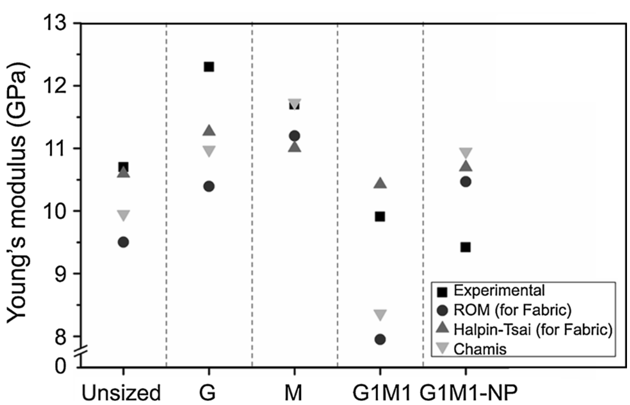

Fig. 5 Comparison of experimental Young's modulus with those calculated by different theoretical models (ROM, H–T and Chamis models) (sample codes are according to Table 1)

failure is observed. On the other hand, fiber pull-outs with different lengths are observed in G, G1M1 and G1M1-NP samples, indicating a strong interfacial contribution through out-force application. The amount of energy absorption or toughness of composites is related to the type of fiber failure. When the fibers were pulled out, the matrix roughness, interaction between the functional groups of the fiber surface and matrix, and the bridging effect of silica nanoparticles caused the composite to absorb much more energy rather than fibers to fracture. The more energy absorption capacity observed was due to the debonding, stretching, and fiber pull-out [45, 46]. Thus, as shown in Fig. 2b, d, e, these samples absorb much more energy in equal volume fractions than the other fiber-reinforced composites.

Figure 3 shows the SEM micrographs of the specimens fractured after tensile test. A same trend can be observed in the SEM micrographs as shown above. The samples reinforced with unsized fiber show a catastrophic failure. In other words, a sudden rupture occurred at the interface and the bulk of matrix, wherein the extraction of fiber was the dominant mechanism (Fig. 3b, d, e). Nevertheless, as it can be seen, the surface of the fibers is not smooth. In other words, the derbies and residues on the fiber surfaces in G and G1M1-NP samples are much greater, indicating the symbiosis of physical and chemical interactions at the interface. Furthermore, Fig. 3d shows a bundle of fibers instead of a single fiber pull-out, indicating that the fibers are packed with epoxy resin through modifiers. Although the fiber is pulled out in the sample M (Fig. 3c), the fiber surface is approximately clean, confirming poor interactions. In the sample M, such observations were also validated by the gaps existing at the fiber–matrix interface. As shown in Fig. 3e, the nanosilica particles present at the interface can act as anchors, resulting in better stress-transferring process.

Figure 4a shows the plot of the experimentally determined Young's modulus versus the parameters calculated by the ROM equations. It is clear that there is a significant difference between the ROM values estimated for the longitudinal (E_1) and transversal (E_2) Young's moduli (for UD composites), and the Young's moduli values determined experimentally. In the calculation of UD composites properties, the ROM equations gave upper (E_1) and lower bound (E_2) results. After modification of ROM equations for woven fabric lamina, a good correlation between the experimental and calculated elastic modulus data was obtained.

Figure 4b displays the plot of the data obtained experimentally and those calculated according to H–T equations. For the woven fabric lamina, a correlation function was calculated based on the differences between the experimental and calculated values and applied to the H–T values to reduce their differences with the experimental data.

Figure 5 shows the comparison of experimental Young's modulus with those calculated by different theoretical models (ROM, H–T and Chamis models). For the unsized, G and G1M1 samples, the H–T model shows the best agreement with the experimental results. An excellent agreement between the values predicted by the Chamis equation and the experimental data of the M sample can be also observed in this figure. In G1M1-NP sample, the results obtained from the ROM model are close to those observed

Table 5 Shear properties of glass fabric/epoxy composite panels

Sample code	Shear strength (MPa)	Shear modulus (GPa)	Toughness (N mm)
Unsized	51.90 ± 1.28[a]	1.10 ± 0.11[A]	532.62 ± 18.64
G	70.73 ± 1.81[c]	1.36 ± 0.15	1778.00 ± 53.35
M	56.03 ± 2.88[a, b]	1.17 ± 0.09	1029.78 ± 25.74
G1M1	58.88 ± 0.92[b]	0.98 ± 0.1	543.77 ± 16.92
G1M1-NP	76.60 ± 2.97[d]	1.340 ± .12	2671.84 ± 68.92

[a,b,c,d,e] Means with the same superscript are not statistically different ($P < 0.05$)

[A] Mean ± Std. deviation

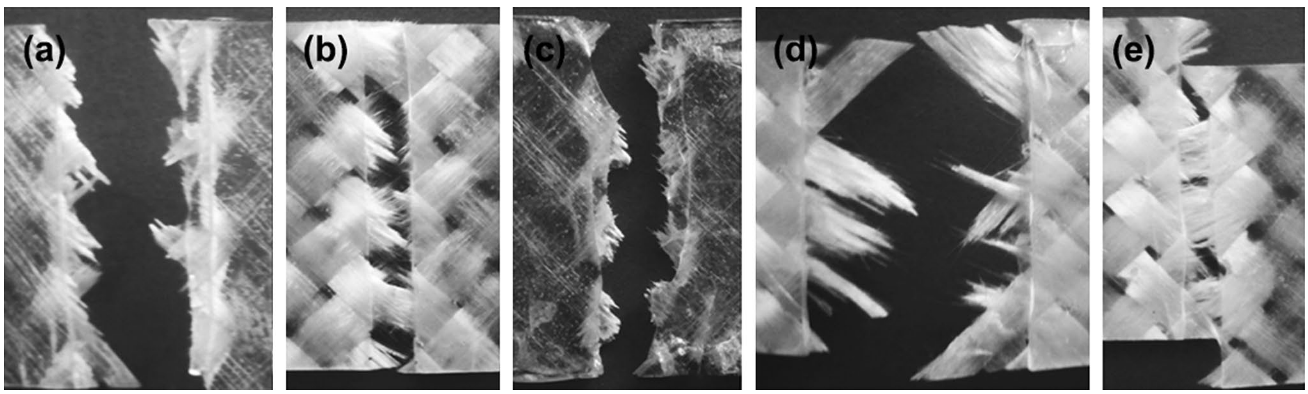

Fig. 6 Fracture type after shear testing for samples: **a** unsized, **b** G, **c** M, **d** G1M1, and **e** G1M1-NP (sample codes are according to Table 1)

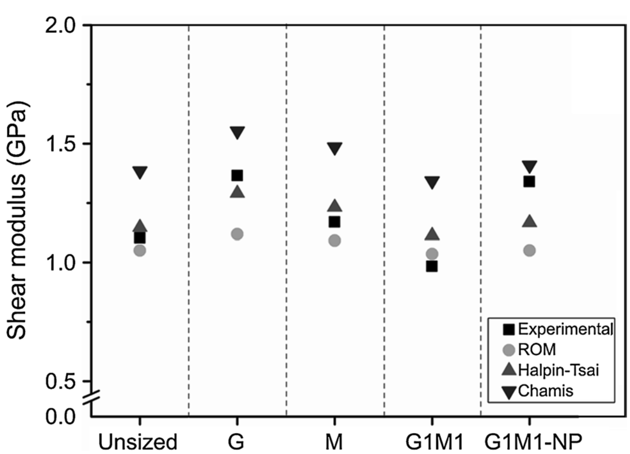

Fig. 7 Comparison of experimental shear modulus with those calculated by different theoretical models (ROM, H–T and Chamis models)

in the experiments. However, a deviation of 11% was found between the theoretical and experimental values. The presence of voids in the matrix might affect the experimental data.

Shear properties of composite panels

Shear strength and toughness results of the epoxy composite panels reinforced with the unsized- and silane-treated glass fabrics are presented in Table 5. All results were normalized based on the highest fiber volume fraction of composite specimens (24%, Table 3). One-way analysis of variance (ANOVA) and Duncan's test were used for the analysis of the experimental results ($P < 0.05$).

The G1M1-NP sample showed a superior improvement in both shear strength and toughness under in-plane shear testing, as it exhibited an increase of around 8 and 50% in the strength and toughness values, respectively, in comparison with the sample G. The incorporation of silica nanoparticles in the sizing dramatically modified the fiber surface texture, and improved the toughness value up to 3.91 times higher than that of the sample G1M1. The addition of SiO_2 nanoparticles in the silane blend significantly changed the fiber surface morphology, modified the mode of failure, and allowed the fracture to follow a torturous path along the interphase, causing more energy to be absorbed.

Figure 6 shows damage modes of the sectioned specimen after the test for the composites treated with different sizing mixtures. The unsized and *M* samples exhibit a brittle behavior (Fig. 6a, c). The G1M1 sample shows a progressive failure including fiber failure and debonding (splitting) (Fig. 6d). The G and G1M1-NP samples are not completely separated into two pieces, since fibers bridged the gap and held the pieces together (Fig. 6b, e). This mode of failure is associated with high-energy absorption (or toughness) [47].

This result is also in agreement with the data presented in Table 5.

Figure 7 shows the comparison of the experimental shear modulus with those calculated by different theoretical models (ROM, H–T and Chamis models). The shear modulus values calculated by the H–T equations show a good agreement with the experimental values.

Conclusion

In this paper, the effect of texture and chemical bonding on the fiber–matrix interphase using a model sizing system comprised of only silane-coupling and roughening agents was studied. The number of the reactive sites, which bonded the epoxy molecules on the fiber surface, was controlled by the silane chemistry. Binary coupling agents including a silane reactive to epoxy group (GPS) and a non-reactive silane (MPS), as well as silica nanoparticles as roughening agents were chosen for fiber surface modification. The results demonstrated the benefit of employing both chemical bonding and texturing for improving both tensile strength and toughness of composites. Glass fabrics treated with sizing mixtures based on colloidal silica particle suspensions and the blend of silane-coupling agents showed enhanced interfacial adhesion. A simultaneous improvement of both tensile strength and toughness was observed for the epoxy composite reinforced with the hybrid-sized glass fiber including silane mixtures and nanosilica. In fact, incorporation of colloidal silica within the hybrid sizing mixtures dramatically modified the fiber surface texture and created mechanical interlocking between the glass fabric and resin. Consequently, the toughness of G1M1-NP sample could be improved to 3.91 times higher in comparison with that of the G1M1 sample. The failure behavior studied by SEM technique displayed the cracks in a tortuous path in the hybrid sizing system, resulting in higher energy absorption and toughness. A mathematical analysis was performed on the experimental data. The rule of mixtures (ROM), Halpin–Tsai (H–T), and Chamis equations were used in the study, because they are the most widely used equations reported in literature. The elastic and shear moduli of composites were considered as the controlling parameters. It was found that the ROM model provided approximate values for the studied parameters, representing upper bound values for the elastic modulus. In G1M1-NP sample, the elastic modulus values calculated by the ROM equations were in good agreement with those obtained from the experiments. The shear modulus values calculated according to the H–T equations were close to the experimental shear modulus values. A correlation function was calculated based on the differences between the experimental and calculated values and applied to the H–T values to reduce their differences with the experimental data.

References

1. Adloo A, Sadeghi M, Masoomi M, Pazhooh HN (2016) High performance polymeric bipolar plate based on polypropylene/graphite/graphene/nano-carbon black composites for PEM fuel cells. Renew Energy 99:867–874
2. Nunna S, Naebe M, Hameed N, Fox BL, Creighton C (2017) Evolution of radial heterogeneity in polyacrylonitrile fibres during thermal stabilization: an overview. Polym Degrad Stab 136:20–30
3. Pazhooh HN, Bagheri R, Adloo A (2017) Fabrication of semiconductive natural rubber nanocomposites with low copper nanoparticle contents. Polymer 108:135–145
4. Shokrieh MM, Kashani ARS, Mosalmani R (2016) A dynamic constitutive-micromechanical model to predict the strain rate-dependent mechanical behavior of carbon nanofiber/epoxy nanocomposites. Iran Polym J 25:487–501
5. Safi S, Zadhoush A, Masoomi M (2016) Effects of chemical surface pretreatment on tensile properties of a single glass fiber and the glass fiber reinforced epoxy composite. Polym Compos 37:91–100
6. Daryadel S, Ray C, Pandya T, Mantena P (2015) Energy absorption of pultruded hybrid glass/graphite epoxy composites under high strain-rate SHPBcompression loading. Mater Sci Appl 6:511–518
7. Garg M, Sharma S, Mehta R (2017) Role of curing conditions and silanization of glass fibers on carbon nanotubes (CNTs) reinforced glass fiber epoxy composites. Compos Interface 24:233–253
8. Moallemzadeh AR, Sabet AR, Abedini H (2017) Mechanical and morphological study of polymer composite plates having different fiber surface treatments with particular response to high velocity projectile impact. Iran Polym J 26:229–238
9. Kim HH, Kim SY, Kim DH, Oh CY, Jo NJ (2014) Effect of silane coupling agent on the flexural property of glass fiber reinforced composite film. J Mater Sci Chem Eng 2:38–42
10. Ahmad T, Raza SS, Aleem E, Kamran M, Manzoor U, Makhdoom A, Ahmad R, Mukhtar S (2017) Improvement in mechanical and thermal properties of unsaturated polyester-based hybrid composites. Iran Polym J 26:305–311
11. Gao A, Gu Y, Wu Q, Yuan C, Li M, Zhang Z (2015) Influence of processing temperature on interfacial behavior of HKT800 carbon fiber with BMI and epoxy matrices. Chin J Aeronaut 28:1255–1262
12. Kim JK, Mai YW (2006) Engineered interfaces in fibre reinforced composites: surface treatment of fibers and effects on composite properties, 1st edn, Chap 5. Elsevier, Kidlington
13. Debeli DK, Guo J, Li Z, Zhu J, Li N (2017) Treatment of ramie fiber with different techniques: the influence of diammonium phosphate on interfacial adhesion properties of ramie fiber-reinforced polylactic acid composite. Iran Polym J 26:341–354
14. Gao X, Jensen RE, McKnight SH, Gillespie JW Jr (2011) Effect of colloidal silica on the strength and energy absorption of glass fiber/epoxy interphases. Compos A 42:1738–1747
15. Islam MK, Sharif A (2016) Nanocharacterization of interface between natural fiber and polymer matrix: an overview. Compos Interface 23:105–123
16. Moosburger-Will J, Jäger J, Strauch J, Bauer M, Strobl S, Linscheid FF, Horn S (2016) Interphase formation and fiber matrix adhesion in carbon fiber reinforced epoxy resin: influence of carbon fiber surface chemistry. Compos Interface 24:691–710

17. Xia X, Liu W, Zhou L, Hua Z, Liu H, He S (2016) Modification of flax fiber surface and its compatibilization in polylactic acid/flax composites. Iran Polym J 25:25–35
18. Bagheri MR, Vanini SAS, Kordani N, Sadighi M (2015) The effect of nanoparticles in single-lap composite joints studied by experimental and numerical analyses. Iran Polym J24:629–640
19. Kuzmin KL, Timoshkin IA, Gutnikov SI, Zhukovskaya ES, Lipatov YV, Lazoryak BI (2017) Effect of silane/nano-silica on the mechanical properties of basalt fiber reinforced epoxy composites. Compos Interface 24:13–34
20. Sever K, Sarikanat M, Seki Y, Tavman IH (2009) Concentration effect of glycidoxypropyltrimethoxysilane on the mechanical properties of glass fiber-epoxy composites. Polym Compos 30:1251–1257
21. Yang L, Thomason JL (2013) Effect of silane coupling agent on mechanical performance of glass fibre. J Mater Sci 48:1947–1954
22. Dey M, Deitzel JM, Gillespie JW, Schweiger S (2014) Influence of sizing formulations on glass/epoxy interphase properties. Compos Part A 63:59–67
23. Gao X, Jensen RE, Li W, Deitzel J, Mcknight SH, Gillespie JW Jr (2008) Effect of fiber surface texture created from silane blends on the strength and energy absorption of the glass fiber/epoxy interphase. J Compos Mater 42:513–534
24. Jensen RE, McKnight SH (2006) Inorganic–organic fiber sizings for enhanced energy absorption in glass fiber-reinforced composites intended for structural applications. Compos Sci Technol 66:509–521
25. Duan J, Kim C, Jiang P, Wang G (2010) Nano-AlN functionalization by silane modification for the preparation of covalent-integrated epoxy/poly(ether imide) nanocomposites. J Appl Polym Sci 115:2734–2746
26. Lee CY, Bae JH, Kim TY, Chang SH, Kim SY (2015) Using silane-functionalized graphene oxides for enhancing the interfacial bonding strength of carbon/epoxy composites. Compos A 75:11–17
27. Yang P, Wang G, Xia X, Takezawa Y, Wang H, Yamada S, Du Q, Zhong W (2008) Preparation and thermo-mechanical properties of heat-resistant epoxy/silica hybrid materials. Polym Eng Sci 48:1214–1221
28. Safi S, Zadhoush A, Ahmadi M (2017) Flexural and Charpy impact behaviour of epoxy/glass fabric treated by nano-SiO_2 and silane blend. Plast Rubber Compos 46:314–321
29. Paiva JMF, Santos ADN, Rezende MC (2009) Mechanical and morphological characterizations of carbon fiber fabric reinforced epoxy composites used in aeronautical field. Mater Res 12:367–374
30. Gay D (2015) Composite materials: design and applications, Third Edition, Chapter 3. CRC Press, Taylor & Francis Group, Boca Raton
31. Younes R, Hallal A, Chehade FH, Fardoun F (2012) Comparative review study on elastic properties modeling for unidirectional composite materials. In: Hu N (ed) Composites and their properties. Intech, Open Access Publisher
32. Mallick PK (2008) Fiber reinforced composites: materials, manufacturing, and design, Chapter 3. CRC Press, Taylor & Francis Group, LLC, Boca Raton
33. Abdel Ghafaar M, Mazen AA, El-Mahallawy NA (2006) Application of the rule of mixtures and Halpin–Tsai equations to woven fabric reinforced epoxy composites. J Eng Sci 34:227–236
34. Reilly SP, Thomason JL (2010) Effects of silane coating on the properties of glass fibre and glass fibre reinforced epoxy resin. In: Paper presented at the 14th European conference on composite materials, Budapest
35. Defense UDO (1999) Composite materials handbook-MIL 17: guidelines for characterization of structural materials. Taylor & Francis, Boca Raton
36. Naebe M, Abolhasani MM, Khayyam H, Amini A, Fox B (2016) Crack damage in polymers and composites: a review. Polym Rev 56:31–69
37. Lee SO, Choi SH, Kwon SH, Rhee KY, Park SJ (2015) Modification of surface functionality of multi-walled carbon nanotubes on fracture toughness of basalt fiber-reinforced composites. Compos Part B 79:47–52
38. Yu B, Geng C, Zhou M, Bai H, Fu Q, He B (2016) Impact toughness of polypropylene/glass fiber composites: interplay between intrinsic toughening and extrinsic toughening. Compos B 92:413–419
39. Ahmadi M, Zahibi O, Masoomi M, Naebe M (2016) Synergistic effect of MWCNTs functionalization on interfacial and mechanical properties of multi-scale UHMWPE fibre reinforced epoxy composites. Compos Sci Technol 134:1–11
40. Karger-Kocsis J, Mahmood H, Pegoretti A (2015) Recent advances in fiber/matrix interphase engineering for polymer composites. Prog Mater Sci 73:1–43
41. Esmizadeh E, Yousefi AA, Naderi G (2015) Effect of type and aspect ratio of different carbon nanotubes on cure behavior of epoxy-based nanocomposites. Iran Polym J 24:1–12
42. Barikani M, Saidpour H, Sezen M (2002) Mode-I interlaminar fracture toughness in unidirectional carbon-fibre/epoxy composites. Iran Polym J 11:413–423
43. Ghorabi S, Rajabi L, Madaeni SS, Zinadini S, Derakhshan AA (2012) Effects of three surfactant types of anionic, cationic and non-ionic on tensile properties and fracture surface morphology of epoxy/MWCNT nanocomposites. Iran Polym J 21:121–130
44. Shokrieh MM, Esmkhani M, Vahedi F, Shahverdi HR (2013) Improvement of mechanical and electrical properties of epoxy resin with carbon nanofibers. Iran Polym J 22:721–727
45. Razavi Nouri M, Morshedian J (1995) Tensile and flexural behaviour of fibre reinforced cementitious composites. Iran J Polym SciTechnol 4:56–63
46. Najafi M, Khalili SMR, Eslami-Farsani R (2014) Hybridization effect of basalt and carbon fibers on impact and flexural properties of phenolic composites. Iran Polym J 23:767–773
47. Sawpan MA, Pickering KL, Fernyhough A (2011) Improvement of mechanical performance of industrial hemp fibre reinforced polylactide biocomposites. Compos A 42:310–319